

Visualizations of sound energy across coupled rooms using a diffusion equation model

Yun Jing and Ning Xiang

Graduate Program in Architectural Acoustics, School of Architecture, Rensselaer Polytechnic Institute, Troy,
New York 12180
xiangn@rpi.edu; jingy@rpi.edu

Abstract: Visualizations, based on a diffusion equation model, are presented for both steady-state and transient sound energy. For steady-state sound-pressure level distributions, animations created by scanning from the primary room to the secondary room reveal discontinuous transitions of sound energy caused by a location change from the wall area to the aperture area. Animations of time-dependent energy flow directions visualize the energy flows across coupled spaces. This study also reveals a “reversal” characteristic of energy flow directions which seems to be dependent on the size and location of the aperture.

© 2008 Acoustical Society of America

PACS numbers: 43.55.Br, 43.55.Ka [DKW]

Date Received: April 6, 2008 Date Accepted: September 5, 2008

1. Introduction

Acoustics in coupled spaces has been gaining a wide interest due to its ability to create non-exponential energy decay resulting from energy exchange at an aperture coupling multiple spaces. Coupled chambers have already been built in some concert halls to attach to the main hall, in order to produce a double-sloped energy decay, which has a fast decay at the beginning and a slow decay at the tail. This specific decay profile has been considered to be beneficial for both perceived clarity and reverberance.

The objective of this paper is to visualize sound-pressure distributions and sound energy flows. Most recently, a diffusion equation model has been applied to acoustically coupled spaces. Its validity has been experimentally substantiated.¹ The diffusion equation model for room-acoustic predictions was first validated by Picaut *et al.*² and has been recently extended in room-acoustics applications, mainly to various types of single-volume spaces.²⁻⁶

The previous work on the diffusion equation model in acoustically coupled rooms¹ has not considered sound-energy flows in coupled spaces. Energy flow is of significant importance since a double-sloped energy decay is caused by energy flow feedback: when sound energy in the primary room decays to a certain level, the slower decreasing, but higher energy in the secondary room flows back to the primary room and dominates the decay. While in previous literature steady-state figures are of the majority, the aim of this work is to visualize sound-pressure distributions and the sound-energy flows across the coupling aperture of two coupled rooms.

2. Diffusion equation model for room-acoustic prediction

Given the slow rates of energy change with time, according to Fick's law, the gradient of the sound-energy density $w(\mathbf{r}, t)$ at position \mathbf{r} and time t in the room under investigation causes the sound-energy flow vector \mathbf{J} ,^{2,3}

$$\mathbf{J} = -D \text{grad } w(\mathbf{r}, t), \quad (1)$$

where $D = \lambda c / 3$ is defined as the diffusion coefficient, with λ being the mean-free path. The expression in Eq. (1) follows a physical analogy with the diffusion of particles in a scattering medium.² It implicitly assumes sound particles traveling along straight lines at sound speed c in the room under investigation with diffusely reflecting walls. In a region without sound sources,

a change of the sound energy density per unit time is associated with changes in the sound-energy flow vector,

$$\frac{\partial w(\mathbf{r}, t)}{\partial t} = -\operatorname{div} \mathbf{J} = D\nabla^2 w(\mathbf{r}, t). \quad (2)$$

The sound-energy density is then governed by the diffusion equation

$$\frac{\partial w(\mathbf{r}, t)}{\partial t} - D\nabla^2 w(\mathbf{r}, t) + cmw(\mathbf{r}, t) = q(\mathbf{r}, t) \quad \in V, \quad (3)$$

where the subroom, denoted by domain V with a source term $q(\mathbf{r}, t)$, is zero for any subdomain where no source is present. The term $cmw(\mathbf{r}, t)$ accounts for air dissipation in the room(s),⁷ and can be extended to account for absorption due to scattering objects inside the room(s).⁴ Equation (3) is the interior equation in domain V , being subject to the boundary condition on the interior surface S ,

$$D \frac{\partial w(\mathbf{r}, t)}{\partial n} + \frac{c\alpha}{2(2-\alpha)} w(\mathbf{r}, t) = 0. \quad (4)$$

Jing and Xiang⁶ have demonstrated that the diffusion equation with this boundary condition can model surfaces with absorption coefficients ranging from 0 to 1.0.

In modeling coupled rooms, the domain V comprises an arbitrary number of subdomains, which are the subrooms of the coupled-room system. Diffusion coefficients for each subroom are assigned based on the mean-free path of each subroom under the assumption that coupling these subrooms does not significantly change their free-path distributions.¹ Coupling configurations with weak coupling (small coupling apertures) approximately meet this assumption.

3. Sound pressure and energy flow distributions

An inherent advantage of the diffusion equation model is its ability to model sound-energy density at all locations within the space with a computational load on the order of minutes on a current personal computer. The gradient of the sound-energy density expressed in Eq. (1) then can be obtained. Therefore, the diffusion equation model is intrinsically suitable for modeling the sound-pressure level distribution as well as the energy flows. This section presents the animations of both steady sound-pressure level distributions and time-dependent energy flows.

3.1 Coupled-room description

Figure 1(a) illustrates the geometry of the coupled-room system as defined within a Cartesian coordinate system. The aperture is a square with a width of 3 m, and spans from $y=0.32$ m to $y=3.32$ m. The smaller room is the primary room with an acoustic source located at $(-5, 2.4, 1.3)$ m. Three different sets of absorption coefficients are assigned to the primary room and the secondary room, to obtain three configurations of the natural reverberation times (RTs) of both rooms, which cover the cases where the natural reverberation time T_1 of the primary room is smaller, the same as, and larger than the natural reverberation time T_2 of the secondary room, respectively. Table 1 lists relevant parameters. The purpose of using these configurations is to explore the relationship between the energy flow and each room's natural reverberation times.

3.2 Sound-pressure level distributions

In a previous study,¹ the sound-pressure level distributions along a line drawn perpendicularly across the aperture have been studied both experimentally and numerically. In this study, we provide more insight into the sound-pressure level distribution parallel to the aperture and the

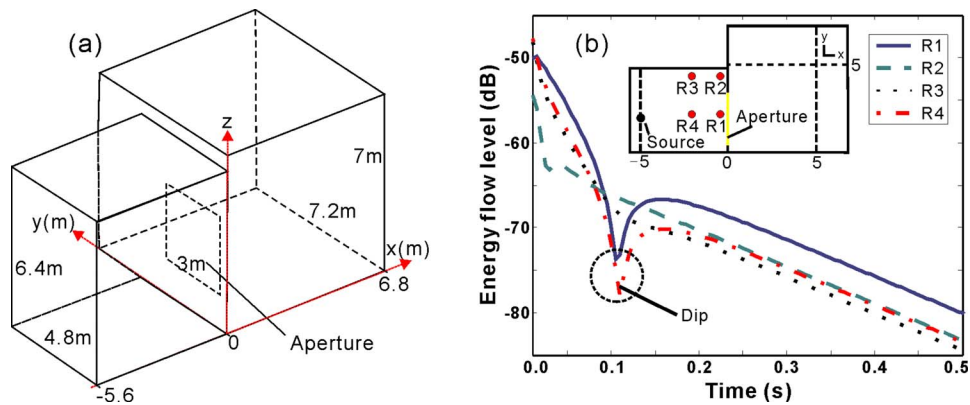


Fig. 1. (Color online) (a) Dimensions and coordinate definition of the two coupled rooms. (b) Energy-flow decays in the primary room for case 1 ($T_1 < T_2$).

wall containing the aperture, starting from a location near the aperture to a location far away from the aperture. The transition of the sound-pressure level caused by the location changing from the aperture opening to the wall is of particular interest.

All three room configurations are included in the investigation of the sound-pressure level distributions. The sound source has a power of 0.01 W. The diffusion equation is solved by a commercial finite element solver with approximately 8000 meshes which fulfills the mesh condition determined by the mean-free path length.³ The direct sound field is excluded,³ leaving only the reverberant sound field. The animations show the sound-pressure level distributions scanning from $x = -2$ m to $x = 2$ m (i.e., from the primary room to the secondary room), at a height of 3 m. Multimedia 1 represents case 1 as listed in Table 1. To highlight the continuity of the sound-pressure level distributions across the aperture, the sound-pressure level distribution at $x = -0.05$ m holds on in the animations while the scanning goes further into the secondary room.

Mm. 1. Sound-pressure level distribution from the primary room (4.8 m wide) to the secondary room (7.2 m wide) for case 1 ($T_1 < T_2$). The last sound-pressure level distribution in the primary room (at $x = -0.05$) holds on while the scanning goes further into the secondary room to highlight the continuity of the distribution at the aperture. This is a file of type “avi” (304 Kb).

To save space, the animations for cases 2 and 3 are not included in this paper. However, all three animations show the sound-pressure continuity from the primary room to the secondary room across the aperture and the noncontinuous transition in each room from the wall to the opening area when the receivers get close to the aperture. Experimental verifications have been undertaken and will be reported in a follow-up paper.

Table 1. Values of absorption coefficients and natural reverberation times in two rooms

| | Case 1 | Case 2 | Case 3 |
|--------------|--------|--------|--------|
| α_1^a | 0.2 | 0.2 | 0.2 |
| α_2 | 0.1 | 0.25 | 0.60 |
| T_1/s^b | 0.66 | 0.66 | 0.66 |
| T_2/s | 1.78 | 0.66 | 0.20 |

^a1 represents the main room, 2 represents the secondary room.

^bThe RTs are estimated by the Eyring equation.

3.3 Energy flows

To calculate the time-dependent energy flow, an impulsive sound energy is generated by the acoustic source to excite the room. The time step is set to 5 ms, and the modeling time is from 10 to 150 ms for the three cases listed in Table 1. The diffusion equation model is not valid within the “mean-free time,”³ which is around 0 to 10 ms in this configuration. After 150 ms, the energy flows do not change significantly for all three cases. The time-dependent energy flows are determined using Eq. (1). Multimedia 2 provides three-dimensional (3D) energy flow distributions for case 1. The 3D arrows show the direction of the energy flow. For the purpose of clarity, Mm. 3 and 4 illustrate case 1 and case 2 in a two-dimensional representation where energy flows are presented on the xy -plane at a height of $z=3$ m.

Mm. 2. Three-dimensional time-dependent sound-energy flow for case 1 ($T_1 < T_2$). This is a file of type “avi” (2.4 Mb).

Mm. 3. Two-dimensional time-dependent sound-energy flow for case 1 ($T_1 < T_2$). This is a file of type “avi” (2.2 Mb).

Mm. 4. Two-dimensional time-dependent sound energy flow for Case 2 ($T_1 = T_2$). This is a file of type “avi” (1.8 Mb).

For case 1, where the natural RT in the primary room is smaller than that in the secondary room, Mm. 2 shows a clear energy feedback near the aperture beginning at around 110 ms in terms of the energy flow directions, i.e., the sound-energy flows from the secondary room into the primary room via the aperture. In addition, the start of the energy feedback appears earlier around the aperture than it does at a location further inside the secondary room. This delay in energy feedback inside the secondary room is probably due to the fact that the primary room draws the sound energy from the secondary room faster at the position near the aperture (i.e., near the primary room). For the other two cases, no apparent energy feedback from the secondary room can be found, especially in case 3, where the RT of the secondary room is much smaller than the primary room. However, the animation for case 3 also has not been included in order to minimize the number of animations. For case 2, in the proximity of the source, reversal of flow directions occurs. Additional simulations show that this phenomenon also occurs in single rooms. In a single room, initially when the energy decays from an impulse, the energy is strongest around the source and the energy flows point away from the source. As time progresses, the region with the strongest energy moves from the source to the other place (usually not far away from the source) in the room and stays steady, indicating that the energy flow now points outwards from a different spot, which is the reason why the energy flow directions reverse. Therefore, the reversal in flow direction near the source probably has little relevance to the energy feedback through the aperture from the coupled room. Although it seems plausible that the energy flow in case 2, when $T_1 = T_2$, shows a trend going back to the primary room at the aperture area, a longer time simulation shows negligible energy feedback around the aperture.

3.4 Energy-flow decays

While the aforementioned animations create visualization of the direction of energy flows, this section elaborates on sound-energy flow decays. Since distinct energy feedback can be demonstrated only in case 1, energy-flow decays are discussed only under this circumstance. The time-dependent decaying function at location \mathbf{r} of energy-flow levels is defined as

$$J_L(\mathbf{r}, t) = 10 \log \left[\left(\frac{\partial w(\mathbf{r}, t)}{\partial x} \right)^2 + \left(\frac{\partial w(\mathbf{r}, t)}{\partial y} \right)^2 + \left(\frac{\partial w(\mathbf{r}, t)}{\partial z} \right)^2 \right]^{1/2}, \quad (5)$$

with the diffusion coefficient D being neglected, because the relative levels of the energy flow in each room are of major concern.

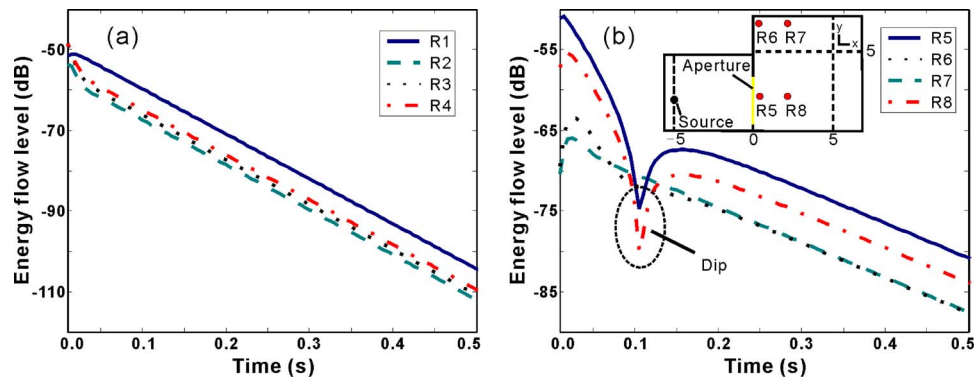


Fig. 2. (Color online) (a) Energy-flow decays in a single room; in the primary room the aperture is replaced by a wall material with an absorption coefficient 1.0. (b) Energy-flow decays in the secondary room for case 1 ($T_1 < T_2$).

Figure 1(b) illustrates the energy-flow decays in the primary room for case 1. Four positions at R1 $(-0.05, 2.5, 3)$ m, R2 $(-0.05, 4.5, 3)$ m, R3 $(-2, 4.5, 3)$ m, and R4 $(-2, 2.5, 3)$ m are chosen. Distinct “dips” of the energy flows are found for R1 and R4, both being along the line $y=2.5$ m. The energy-flow dips occurs at around 105 and 110 ms, the time at which the energy feedback from the secondary room is about to happen. The dip of the energy-flow level strongly suggests that, in a certain area, the magnitude of the energy flow abruptly drops and rises along a reversal of direction, when the energy feedback happens or is about to happen. Thus, a sharp dip in the energy-flow decay function is formed. For R2 and R3, both along the line at $y=4.5$ m, the energy flows decay monotonously, showing no abrupt transition. Additional simulations show that the dip is more likely to take place between $y=0.1$ m and $y=4$ m, provided that the receiver position is not too close to the source. Notice that the aperture ranges from $y=0.3$ m to $y=3$ m, implying that the energy-flow dip area (refers to the area where the flow dips occur) is dependent on the aperture size and location. Moreover, the flow direction reversal is most intense along the line $y=2$ m, which is approximately the center line of the aperture. The energy flow at R1 decays rapidly before the dip, and has the largest energy-flow amplitude after the reversal, which has occurred because R1 is in the vicinity of the aperture.

To demonstrate that the reversal characteristic of the energy-flows around the opening region is uniquely associated with coupled spaces, the energy-flow decays are also presented here for a single room where the aperture on the primary-room side is replaced by a wall surface with an absorption coefficient of 1.0 without the secondary room. To enable the comparison, the four receivers remain at the same positions as they were in the coupled space scenario. Figure 2(a) illustrates all the energy-flow decays following a similar exponential decay. Therefore, reversal of the energy-flow direction around the opening region does not occur in this single-room case.

Figure 2(b) illustrates the energy-flow decays in the secondary room for the coupled configuration of case 1. Four receiver positions are at R5 $(0.05, 2.5, 3)$ m, R6 $(0.05, 7, 3)$ m, R7 $(2, 7, 3)$ m, and R8 $(2, 2.5, 3)$ m. Among them, R5 and R8 show the reversal characteristic while the other two receiver positions do not. Further simulations show that the energy-flow dip area is larger in the secondary room than it is in the primary room, probably because the secondary room has a larger size than the primary room.

So far, the discussion has focused on the impulse response of the energy-flow decay, to serve the purpose of visualizing the energy feedback. Additional simulations show that the steady-state impulse response of the energy flow decay has slightly different curve in that the dip occurs at different times. Moreover, the steady-state energy flow decay allows the comparison between itself and the steady-state energy decay (Schroeder decay function), which will reveal the relationship between the energy-flow reversal and the energy decay curve transition

from the first decay curve to the second decay curve.

4. Conclusion

In this paper, the diffusion equation model is used to visualize both steady state-sound-pressure level distribution and time-dependent energy flow in two coupled rooms via multimedia animations. The diffusion equation model is briefly reviewed. Because of its high efficiency in calculating the sound-energy density everywhere in the rooms, it can be used to obtain both sound-energy flows and sound-pressure level distributions with a computational load on the order of minutes. Three different absorption configurations are assigned to a coupled-volume system consisting of two rooms connected by a square opening aperture. Three configurations are investigated: the natural reverberation time in the primary room is shorter, the same, and longer than in the secondary room, respectively.

Animations discussed in Sec. 2.2 illustrate sound-pressure level distributions parallel to the wall containing the aperture by scanning from the primary room to the secondary room. Along the lines parallel to the wall containing the aperture, a distinct pressure level discontinuity is found at the edge of the aperture for all three cases. The time-dependent sound-energy flow directions were presented in two- and three-dimensions. When the natural reverberation time of the primary room is shorter than that of the secondary room, the animation clearly shows the energy feedback, especially in regions around the aperture.

This work also studies time-dependent sound-energy flow levels. Simulations discussed in Sec. 3.3 using the diffusion equation model reveal a distinct characteristic of the energy-flow level decay: a dip in the energy-flow decay function associated with reversal of the energy-flow directions. Around the aperture region, the dip of the energy-flow decay occurs at the time when the energy feedback from the secondary room starts to compensate for the energy outflow. Furthermore, the dip characteristic does not happen everywhere, but is rather in some way restricted by the aperture size and location.

Experimental verifications of sound-pressure level distributions for the two coupled rooms will be discussed in detail in a follow-up paper. Future work should include the experimental verification of sound-energy flow distributions, and the relationship between the time when the dip occurs and the time point where the sound-energy decay turns over from the first decay slope to the second decay.

Acknowledgments

The authors would like to thank Dr. Jason Summers for helpful discussions, and Mr. Clemeth Abercrombie for polishing the language.

References and links

- ¹A. Billon, V. Valeau, A. Sakout, and J. Picaut, "On the use of a diffusion model for acoustically coupled rooms," *J. Acoust. Soc. Am.* **120**, 2043–2054 (2006).
- ²J. Picaut, L. Simon, and J. D. Polack, "A mathematical model of diffuse sound field based on a diffusion equation," *Acta Acust. (Beijing)* **83**, 614–621 (1997).
- ³V. Valeau, J. Picaut, and M. Hodgson, "On the use of a diffusion equation for room-acoustic prediction," *J. Acoust. Soc. Am.* **119**, 1504–1513 (2006).
- ⁴V. Valeau, M. Hodgson, and J. Picaut, "A diffusion-based analogy for the prediction of sound fields in fitted rooms," *Acta Acust. (Beijing)*, **93**, 94–105 (2007).
- ⁵Y. Jing, and N. Xiang, "A modified diffusion equation for room-acoustic prediction (L)," *J. Acoust. Soc. Am.* **121**, 3284–3287 (2007).
- ⁶Y. Jing, and N. Xiang, "On boundary conditions for the diffusion equation in room-acoustic prediction: Theory, simulations, and experiments," *J. Acoust. Soc. Am.* **123**, 145–153 (2008).
- ⁷A. Billon, J. Picaut, C. Foy, V. Valeau, and A. Sakout, "Introducing atmospheric attenuation within a diffusion model for room-acoustic predictions," *J. Acoust. Soc. Am.* **123**, 4040–4043 (2008).